JPE 16-1-26

http://dx.doi.org/10.6113/JPE.2016.16.1.249
ISSN(Print): 1598-2092 / ISSN(Online): 2093-4718

Low-frequency Vibration Suppression Control in a Two-mass System by Using a Torque Feed-forward and Disturbance Torque Observer

Qiong Li†, Qiang Xu*, and Ren Wu*

†,*Dept. of Electronic Engineering, Huazhong University of Technology and Science, Wuhan, China

Abstract

Given that elastic connection is often used between motor drives and load devices in industrial applications, vibration often occurs at the load side. Vibration suppression is a crucial problem that needs to be addressed to achieve a high-performance servo-control system. Scholars have presented many strategies to suppress vibration. In this study, we propose a method to diminish vibration by using a torque feed-forward and disturbance torque observer. We analyze the system performance and explain the principle of the proposed vibration suppression method based on the transfer functions of the system. The design of controller parameters is another important issue in practical applications. We accordingly provide a succinct outline of the design specifications based on the coefficient diagram method. Furthermore, we build a model under the Simulink environment and conduct experiments to validate the proposed method. Results show that speed and position vibrations are successfully suppressed by the proposed method.

Key words: Disturbance observer, Permanent-magnet synchronous motor, Torque feed-forward, Vibration suppression

I. INTRODUCTION

In practical industrial applications, shaft couplings are often used in mechanical transmission devices. However, these elastic connections may cause mechanical resonance that severely deteriorates the performance of controllers and induces speed and position vibrations in the control system. Therefore, mechanical resonance in servo drive systems is a crucial problem that needs to be addressed to achieve high-dynamic and high-precision responses for modern servo-control systems.

Many methods are proposed to suppress the vibration in two-inertia systems. A μ-synthesis with a descriptor form representation is described; its use can achieve strong robustness and vibration suppression [1]. A modified speed-loop controller is presented to improve the performance of present speed controllers [2]. Various controller structures are elucidated to reduce torsional vibration, and relative controller parameters are designed according to the inertia ratio and the phase lag in speed loop [3]. A common approximator using a radical basis function network is applied to the speed loop to weaken the vibration [4]. Unlike the traditional disturbance observer, this method features self-tuning capability. Self-adapting fuzzy control can also be utilized to reduce torsional vibration. A neural network is applied to reconcile load speed and torsional torque to decrease the vibration in a two-inertia system [5]. A method based on a sliding-mode fuzzy controller is also applied to suppress the vibration in a two-inertia system [6]. Saarakkala proposed a model-based two-degrees-of-freedom state-space speed-controller design for a two-mass mechanical system [18] and presented a discrete-time polynomial method for parameter identification of two-mass mechanical loads [19]. An immersion and invariance approach is applied to suppress the vibration in two-mass systems [20]. A fuzzy Luenberger observer to ensure that fitting observer closed-loop poles is used for a system with flexible joint [21]. Jong-Sun Ko presented a neural-load torque compensation method to obtain good precision position control [22].

The design of controller parameters is also an important

Manuscript received May 27, 2015; accepted Sep. 8, 2015
Recommended for publication by Associate Editor Bon-Gwan Gu.
†Corresponding Author: powerdsp@hust.edu.cn
Tel: +86-130, Fax: +86-027-8654662, Huazhong Univ. of Sci. & Tech.
*Dept. of Electronic Eng., Huazhong University of Technology and Science, China

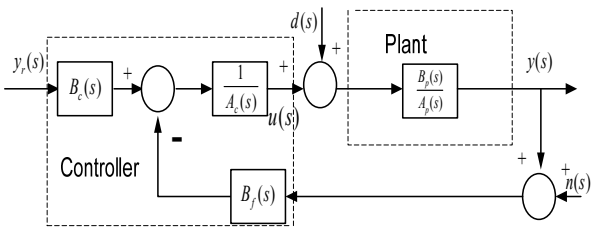

Fig. 1. CDM block diagram.

topic. Complex controllers are generally of high order [7], [8]. However, low-order controllers are more practical in industrial applications. The parameters of high-order controllers are difficult to tune. Therefore, a simple and reliable way to design controller parameters will be useful for practical applications.

Traditional and modern control theories for the design of controller parameters are well known. The polynomial method is another approach to finding approximate parameters for controllers. This method is actually an algebraic design method that uses polynomial expressions. According to the order of the transfer functions of a closed-loop control system and its characteristic polynomial, the coefficients of the controller and polynomial can be calculated by some specifications. Naslin studied the relationship between characteristic ratio and system response in the 1940s [9]. Manabe made a further contribution by proposing the coefficient diagram method (CDM) based on Naslin's theory. CDM successfully solves many controller design problems in practical applications. In this study, we select the CDM to design controller parameters.

This study aims to develop a strategy to suppress the vibration in a two-inertia system and to find a simple and reliable way to design controller parameters. The entire system is expected to have fast response and strong robustness by using the proposed method. Theoretical analysis, simulation, and experimental results are presented to verify the proposed method.

II. PRELIMINARIES

Fig. 1 shows the standard single-input single-output block diagram of CDM, where $A_c(s)$, $B_r(s)$, and $B_f(s)$ are the controller polynomials; y_r, u, d, and n are the input reference, the control, the disturbance, and the measurement noise variables, respectively. The plant to be controlled is represented by $G(s)$ transfer function given by

$$G(s) = B_p(s)/A_p(s). \tag{1}$$

The command and feedback transfer functions of the controller $G_c(s)$ and $G_f(s)$ are expressed in the following forms:

$$G_c(s) = A_c(s)^{-1} B_c(s) \tag{2a}$$

$$G_f(s) = A_c(s)^{-1} B_f(s) \tag{2b}$$

In this study, $P(s)$ is the characteristic polynomial of the closed-loop system given by

$$P(s) = A_c(s)A_p(s) + B_f(s)B_p(s) \tag{3}$$

Given that only three components $A_c(s)$, $B_r(s)$, $B_f(s)$ are to be designed, only three transfer functions are needed for design. Based on the CDM, the following equations are selected as standard [10]:

$$P(s)y = B_p(s)B_c(s)y_r \tag{4a}$$

$$P(s)y = B_p(s)A_c(s)d \tag{4b}$$

$$P(s)(-u) = B_f(s)B_p(s)d \tag{4c}$$

Equ. (4a) determines the command-response characteristics. Equ. (4b) is for the disturbance rejection characteristics. Equ. (4c) is used to check the robustness. Thus, the three basic equations are taken as system performance specifications in the CDM design. The design of P(s) can satisfy the requirements on Equs. (4b) and (4c), and $B_r(s)$ is tuned to satisfy the specification on Equ. (4a).

We explain the CDM design procedure as follows. Some mathematical relations are first described. The general form of P(s) is given by

$$P(s) = a_n s^n + \ldots + a_1 s + a_0 = \sum_{i=0}^{n} a_i s^i \tag{5}$$

The CDM has two design parameters with respect to characteristic polynomial coefficients; these parameters are the equivalent time constant τ and the stability index γ_i. The relations among τ, γ_i, and a_i are given by

$$\tau = a_1/a_0 \tag{6a}$$

$$\gamma_i = a_i^2/a_{i-1}a_{i+1}, i = 1 \cdots n-1 \tag{6b}$$

[11] stated that "the system of any order can stay stable if all the 4th order polynomials are stable with the margin of 1.12." Hence, the design guides for stability are obtained as follows:

$$\begin{aligned} a_i &> 1.12\left[\frac{a_{i-1}}{a_{i+1}}a_{i+2} + \frac{a_{i+1}}{a_{i-1}}a_{i-2}\right], \\ \gamma_i &> 1.12\left(\frac{1}{\gamma_{i-1}} + \frac{1}{\gamma_{i+1}}\right) \end{aligned} \tag{7}$$

In the CDM, the stability indices are recommended as follows [12], [13]:

$$\gamma_1 = 2.5, \gamma_{n-1} = \gamma_{n-2} = \cdots = \gamma_2 = 2. \tag{8}$$

We then design $A_c(s)$ and $B_f(s)$ based on Equ. (8). The denominator $A_p(s)$ and the numerator $B_p(s)$ polynomials can be denoted as

$$A_p(s) = c_m s^m + c_{m-1}s^{m-1} + \cdots + c_1 s^1 + c_0 \tag{9a}$$

$$B_p(s) = b_n s^n + b_{n-1}s^{n-1} + \cdots + b_1 s^1 + b_0 \tag{9b}$$

Controller polynomials are given by

$$A_c(s) = l_p s^p + l_{p-1}s^{p-1} + \cdots + l_1 s^1 + l_0$$

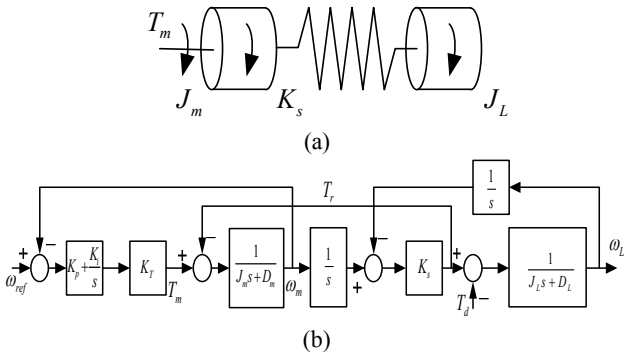

Fig. 2. (a) Mechanical model diagram of a two-inertia system. (b) Classical speed-control diagram of a two-mass system.

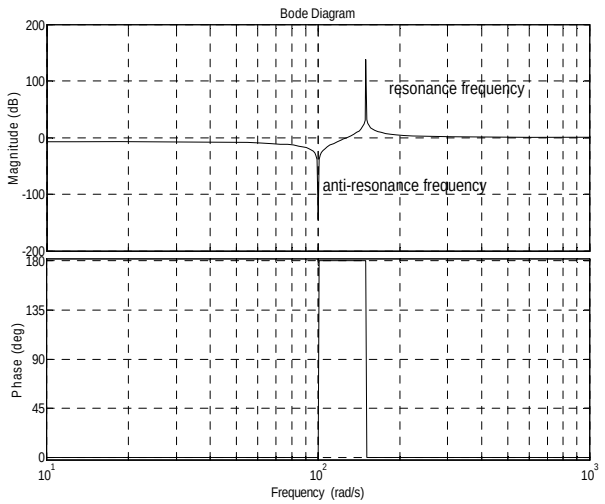

Fig. 3. Response frequency of a two-inertia system.

$$B_f(s) = k_q s^q + k_{q-1} s^{q-1} + \cdots + k_1 s^1 + k_0$$

Equ. (3) can be rewritten as

$$\sum_{i=0}^{n} a_i s^i = \sum_{i=0}^{p} l_i s^i \sum_{i=0}^{m} c_i s^i + \sum_{i=0}^{q} k_i s^i \sum_{i=0}^{n} b_i s^i \qquad (10)$$

where a_i, b_i, and c_i parameters are known. Thus, l_i and k_i can be calculated. Given that $B_r(s)$ is adjusted to satisfy command-response characteristics, we can design it based on practical conditions, as in section IV. B.

III. Mathematical Model of a Two-Inertia System

Fig. 2(a) shows the diagram of a two-inertia system. Fig. 2(b) describes the classical speed-loop-control diagram of a two-inertia system. The definitions of the corresponding parameters are as follows:

J_m *motor inertia*
J_L *load inertia*
D_m *motor viscosity coefficient*
D_L *shaft damping coefficient*
K_T *torque constant*
K_s *shaft stiffness*
ω_{ref} *speed reference*
ω_m *motor speed*
ω_L *load speed*
T_m *electrical torque*
T_d *distance torque*
T_r *torsional torque*

The state equations of the two-inertia system can be written as follows:

$$\begin{aligned}
\frac{d}{dt}\omega_m &= -\frac{D_m}{J_m}\omega_m - \frac{1}{J_m}T_r + \frac{1}{J_m}T_m \\
\frac{d}{dt}T_r &= (K_s - \frac{D_m D_s}{J_m})\omega_m - (K_s - \frac{D_m D_L}{J_L})\omega_L \\
&\quad - D_m(\frac{1}{J_m} + \frac{1}{J_L})T_r + \frac{D_m}{J_m}T_m + \frac{D_m}{J_L}T_L \\
\frac{d}{dt}\omega_L &= -\frac{D_L}{J_L}\omega_L + \frac{1}{J_L}T_r - \frac{1}{J_L}T_L
\end{aligned} \qquad (11)$$

The damping losses assumed to be small can be neglected without affecting the precision of the following analysis significantly. The transfer functions $H_{LM}(s)$, $H_{MM}(s)$, and $H_{RM}(s)$ are as follows:

$$\begin{aligned}
H_{LM}(s) &= \frac{\omega_L(s)}{T_m(s)}|_{T_{d=0}} = \frac{1}{J_L J_m}\frac{K_s}{\Delta(s)} \\
H_{MM}(s) &= \frac{\omega_m(s)}{T_m(s)}|_{T_{d=0}} = \frac{1}{J_L J_m}\frac{J_L s^2 + K_s}{\Delta(s)} \\
H_{RM}(s) &= \frac{T_r(s)}{T_m(s)}|_{T_{d=0}} = \frac{1}{J_L J_m}\frac{J_L K_s s}{\Delta(s)}
\end{aligned} \qquad (12)$$

where $\Delta(s)$ is the characteristic polynomial given by

$$\Delta(s) = s^3 + \frac{K_s(J_m + J_L)}{J_m J_L}s \qquad (13)$$

With further simplification of the above equations, $H_{LM}(s)$ and $H_{MM}(s)$ can be rewritten as

$$H_{MM} = \frac{1}{J_m s}\frac{s^2 + \omega_{ant}^2}{s^2 + \omega_{res}^2} \qquad (14)$$

$$H_{LM} = \frac{1}{J_m J_L s}\frac{K_s}{s^2 + \omega_{res}^2} \qquad (15)$$

where ω_{res} and ω_{ant} are the resonance frequency and the anti-resonance frequency, respectively, defined as

$$\omega_{res} = \sqrt{K_s(\frac{1}{J_m} + \frac{1}{J_L})} \qquad (16)$$

$$\omega_{ant} = \sqrt{\frac{K_s}{J_L}} \qquad (17)$$

Based on Equs. (16) and (17), the increment in the motor inertia decreases the resonance frequency, whereas it has no influence on the anti-resonance frequency. The system performance is seriously damped at the anti-resonance

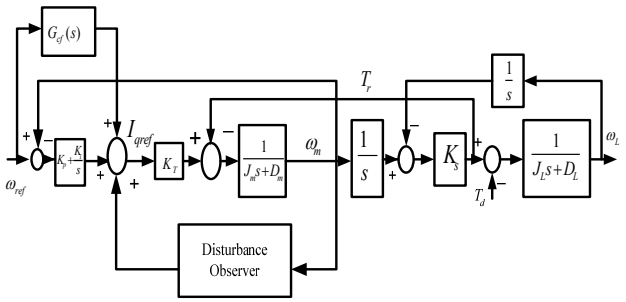

Fig. 4. Diagram of the proposed control strategy for a two-inertia system.

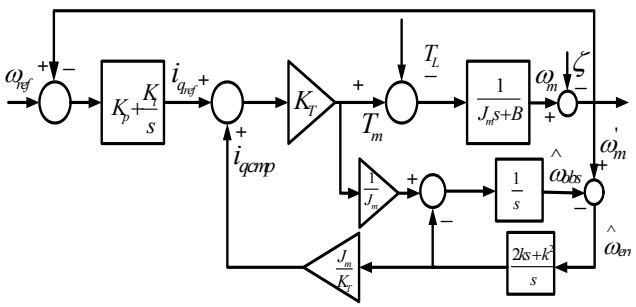

Fig. 5. Disturbance observer.

frequency and has a resonance peak at the resonance frequency. The details from the frequency response of a two-inertia system are presented in Fig. 3. The high gain at the resonance point essentially causes position and speed vibrations. Hence, a method to offset the resonance peak can suppress vibrations.

IV. Vibration Suppression Design

In this section, a method based on a torque feed-forward and disturbance torque observer to suppress the low-frequency vibrations in a two-mass system is proposed. The schematic of the proposed method is shown in Fig. 4. The torque feed-forward compensation is derived from the speed reference, and the disturbance torque observer adopts a low-order observer to estimate the disturbance torque.

The following sections describe the proposed method and the design of controller parameters in detail.

A. Disturbance Observer

Disturbance observer is applied to obtain a robust control system. In this study, we apply a low-order Luenberger observer to estimate the disturbance torque. For simplicity, Fig. 5 shows the principle of the proposed disturbance compensation method. According to Fig. 5, we can obtain the transfer function between T_L and ω_m as Equ. (18). Compared with the transfer function under the traditional proportional–integral (PI) control, which is denoted by Equ. (19), Equ. (18) equals Equ. (19) multiplied by $s^2/(2ks + k^2 – s^2)$. $s^2/(2ks + k^2 – s^2)$ has high-pass filter features. Thus, disturbance torque is seriously damped under the frequency

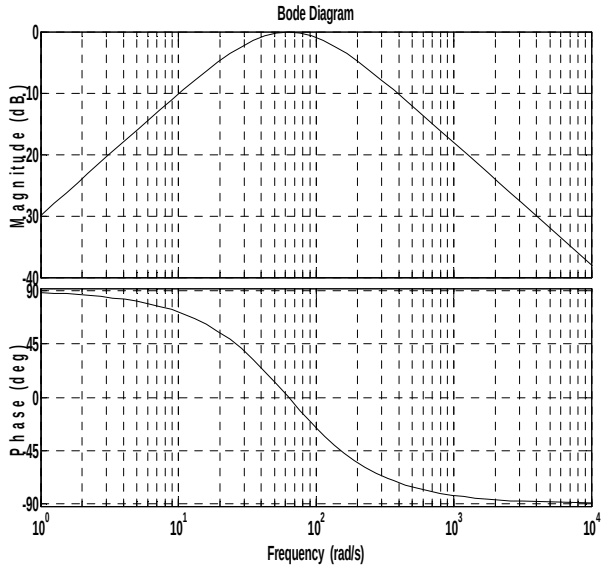

Fig. 6. Bode of Equ. (22) when $K_G = 2\omega_{cf} f, \omega_{cf} = 62.8 rad/s$.

k(*rad/s*). Similarly, the influence of measurement noise on the disturbance observer is damped by a low-pass filter factor $1-J_m(2ks+k^2)s/[K_T(s+k)^2(k_p s+k_i)]$ compared with PI control, that is, Equs. (20) and (21). Therefore, the effect of high-frequency noise can be diminished.

$$-\frac{\omega_m(s)}{T_L(s)} = \frac{s^2}{2ks+k^2-s^2}\frac{s}{J_m s^2 + K_T(K_p s + K_i)} \tag{18}$$

$$-\frac{\omega_{m\text{-}PI}(s)}{T_{L\text{-}PI}(s)} = \frac{s}{J_m s^2 + K_T(K_p s + K_i)} \tag{19}$$

$$\begin{aligned} -\frac{\omega_m(s)}{\zeta(s)} &= \frac{K_T(K_p s+K_i)(s+k)^2 - J_m(2ks+k^2)s}{[J_m s^2 + K_T(K_p s+K_i)](s+k)^2} \\ &= \frac{K_T(K_p s+K_i)}{J_m s^2 + K_T(K_p s+K_i)}\left(1-\frac{J_m(2ks+k^2)s}{K_T(s+k)^2(K_p s+K_i)}\right) \end{aligned} \tag{20}$$

$$-\frac{\omega_{m\_PI}(s)}{\xi_{PI}(s)} = \frac{K_T(K_p s+K_i)}{J_m s^2 + K_T(K_p s+K_i)} \tag{21}$$

According to Equs. (18)-(20), a large k is helpful for disturbance rejection, whereas a small k can improve the capability of measurement noise rejection. Accordingly, k is determined by considering both Equs. (18) and (20). When the system cut-off frequency is near $\sqrt{K_T K_p/(\tau J_m)}$, we recommend that k be not larger than $\sqrt{K_T K_p/(\tau J_m)}$.

B. Parameter Design of Feed-forward Compensator

Calculating torque feed-forward compensation by a classical derivative is usually used. However, classical differentiation is sensitive to noise, thereby limiting its practical application. In this study, we apply Equ. (22) to obtain the torque feed-forward value. We assume that the cut-off frequency is ω_{cf} and the gain is K_G.

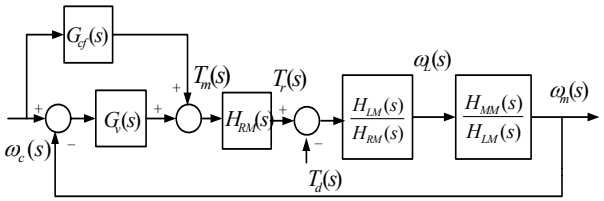

Fig. 7. Control structure of a two-mass system.

$$G_{cf}(s) = \frac{K_G s}{s^2 + 2\omega_{cf} s + \omega_{cf}^2} \tag{22}$$

Fig. 6 shows the frequency response of Equ. (22). From Fig. 6, the response characteristics of Equ. (22) are compatible to the process signals that contain a certain frequency.

The feed-forward compensator procedure is explained hereafter. For simplicity, the transfer function of current loop equals 1 because of the high bandwidth of the current loop, and we assume that $D_M = D_L = 0$. The block diagram of transfer functions is shown in Fig. 7. Given the design of the disturbance observer in section A, we neglect this part to reduce computational effort.

From Fig. 7, the motor speed, the torsional torque, and the electrical torque are represented as

$$\begin{aligned} \omega_m(s) &= H_{SF}(s)\omega_c(s) - H_{TF}(s)T_d(s) \\ T_r(s) &= H_{TS}\omega_c(s) - H_{TL}T_d(s) \\ T_m(s) &= H_{MS}\omega_c(s) - H_{ML}T_d(s) \end{aligned} \tag{23}$$

The transfer functions from the reference speed to the motor speed, from the motor speed to the load torque, the electrical torque to the reference speed, and the torsional torque to the reference speed are described as

$$H_{SF}(s) = \frac{\omega_m(s)}{\omega_c(s)}|_{T_d=0} = \frac{H_{MM}(s)(G_{cf}(s)+G_v(s))}{1+H_{MM}(s)G_v(s)}$$

$$H_{TF}(s) = -\frac{\omega_m(s)}{T_d(s)}|_{\omega_L=0} = \frac{H_{ML}(s)}{1+H_{MM}(s)G_v(s)}$$

$$H_{MS}(s) = \frac{T_m(s)}{\omega_c(s)}|_{T_d=0} = \frac{G_{cf}(s)(1+H_{MM}(s)G_v(s))+G_v(s)}{1+H_{MM}(s)G_v(s)}$$

$$H_{TS}(s) = \frac{T_r(s)}{\omega_c(s)}|_{T_d=0} = \frac{H_{RM}(G_{cf}(s)+G_v(s))}{1+H_{MM}(s)G_v(s)}$$

Thus, the characteristic polynomial can be derived from the above equations.

$$\begin{aligned} \Delta N(s) &= J_m s^4 + K_P s^3 + (J_m\omega_{res}^2 + K_I)s^2 \\ &\quad + K_P\omega_{ant}^2 s + K_I\omega_{ant}^2 \\ &= a_4 s^4 + a_3 s^3 + a_2 s^2 + a_1 s + a_0 \end{aligned} \tag{24}$$

In this section, the CDM that is previously discussed is applied to design control parameters.

According to the discussion in [17], $\gamma_i \geq 2$ is defined for all i = 1,2,...n-1, the step response overshoot is ensured to be small, and a large γ_i leads to great damping. The conclusion can be applied to realize the damping at the resonant frequency by setting an appropriate γ_i. Compared with all-pole systems, two-inertia systems require a particularly large γ_1 because the characteristic ratios with a low index i have an advantageous effect on frequency-domain specifications. Thus, according to the CDM report, $\gamma_1 = 2.5, \gamma_{n-1} = \gamma_{n-2} = \cdots = \gamma_2 = 2$ is recommended considering rapid response and robustness. The elimination of Equ. (24) by Equ. (6b) is thus expressed as

$$K_P = \frac{5\sqrt{2}J_L\omega_{ant}}{5.5} \tag{25a}$$

$$K_I = \frac{2K_s}{5.5} \tag{25b}$$

The basic idea of the design of $G_{cf}(s)$ is to offset the resonance peak of the command response at the resonance point. According to Fig. 7, we can derive that the transfer function between ω_c and ω_L relates to Equ. (26a).

$$\frac{\omega_L}{\omega_c} = \frac{(G_{cf}(s)+G_v(s))K_s s}{\Delta N(s)} \tag{26a}$$

$$\frac{\left|(G_{cf}(s)+G_v(s))K_s s\right|}{\left|\Delta N(s)\right|}\Big|_{\omega=\omega_{res}} \approx 1 \tag{26b}$$

To decrease the gain at the resonance point, the magnitude of the numerator of Equ. (26a) should equal the magnitude of the denominator as much as possible, that is, Equ. (26b). Therefore, Equ. (27) should be satisfied.

$$\omega_{cf}^2 + 2\omega_{cf}\frac{\sqrt{2}K_s}{5J_L} \approx \omega_{res}^2 \tag{27a}$$

$$\frac{K_I\omega_{cf}^2}{K_G + 2\omega_{cf}K_p + K_I} \approx \omega_{res}^2 \tag{27b}$$

When K_p and K_I are known, ω_{cf} and K_G can be calculated based on Equ. (27). In this study, we use the simulation parameters in Table I to verify the availability of the design specifications, that is, Equs. (25) and (27). According to Table I, $\omega_{ant} = 128 rad/s, \omega_{res} = 141 rad/s$. The controller parameters calculated by Equs. (25)–(27) are shown in Table II. The elimination of Equ. (26) by the parameters in Tables I and II derives the bode diagrams of the command response and the disturbance torque response, as shown in Fig. 8. Fig. 8(a) shows the speed frequency response difference between the proposed method and the classical PI control. On the one hand, the command response gain of the classical PI controller (+15 db) is higher than the gain of the proposed

TABLE I
SIMULATION PARAMETERS

Parameter	Value	Unit
J_m	8e-3	Kg.m^2
J_L	2.3e-3	Kg.m^2
D_m	0.002	N.m/rad
D_L	0.002	N.m/rad
K_T	1	N.m/A
K_s	39.2	N.m/rad

TABLE II
DESIGNED PARAMETERS

Parameter	Value	Unit
K_p	0.4	rad/s
K_I	14	rad/s^2
k	50	rad/s
ω_{cf}	123	rad
K_G	−138	N.m/rad
ω_{ant}	114	rad

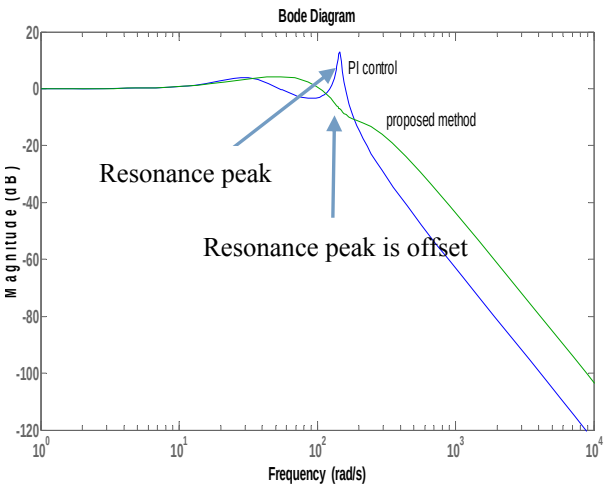

(a)

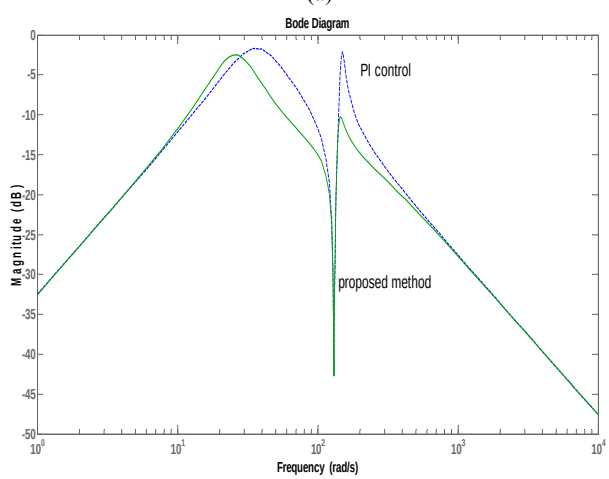

(b)

Fig. 8. (a) Bode diagram of the speed frequency response. (b) Bode diagram of the disturbance frequency response.

method (−9 db) at the resonance frequency. On the other hand, the magnitude of the disturbance frequency response with the proposed method (−12 db) is smaller than that (−3 db) with the classical PI control at the resonance point.

In conclusion, the bode diagrams of the command response and the disturbance response imply the principle of vibration suppression of the proposed method.

V. SIMULATION AND EXPERIMENTAL RESULTS

A. Simulation

Simulations of the PI controller, the PI + disturbance observer controller, and the proposed method controller are conducted. The simulation parameters are the same as those in Table I.

Figs. 9(a)-9(d) show the load speed response, the torsional torque response, the disturbance response, and the position tracking response with three different control systems, respectively. From the curves in Fig. 9(a), a large overshoot (55%) can be found with the PI controller. The vibration in speed lasts for 4 cycles to 5 cycles. The disturbance observer can reduce the vibration (3 cycles) and overshoot (45%), but its performance is not as good as that of the approach proposed in this study. The overshoot is only 12%, and the vibration is almost completely suppressed with the proposed method. The results in Fig. 9(b) indicate that torsional torque is remarkably suppressed by the proposed method, whereas vibration remains for a long time both in the PI controller and the PI + disturbance observer. Fig. 9(c) shows that the disturbance rejection with the PI controller is not as good as those with the other two ways. This result is consistent with the bode diagram in Fig. 8(b). The proposed method has the same disturbance response as the PI + disturbance torque observer because the command torque compensator has no effect on the disturbance rejection capability. Fig. 9(d) describes that the proposed method performs best. The proposed method effectively suppresses vibration and shortens the positioning time in contrast to the PI controller and the PI + disturbance torque observer.

B. Experimental Results

A general picture of the proposed control algorithm is illustrated in Fig. 10 to validate the proposed method. The experimental platform is set up as in Fig. 11. The platform consists of a permanent-magnet synchronous motor (PMSM), a servo driver, a ball screw, and a coupling device, among others. The PMSM parameters are shown in Table III.

The software algorithm of the drive system is designed based on STM32f407. The three different control systems in section V. A are tested for further comparison. The command speed is given in Fig. 12.

When the motor outputs the positioning signal, the sampling of command torque, motor feedback speed, and position error begins. Results are shown in Figs. 13-17. The

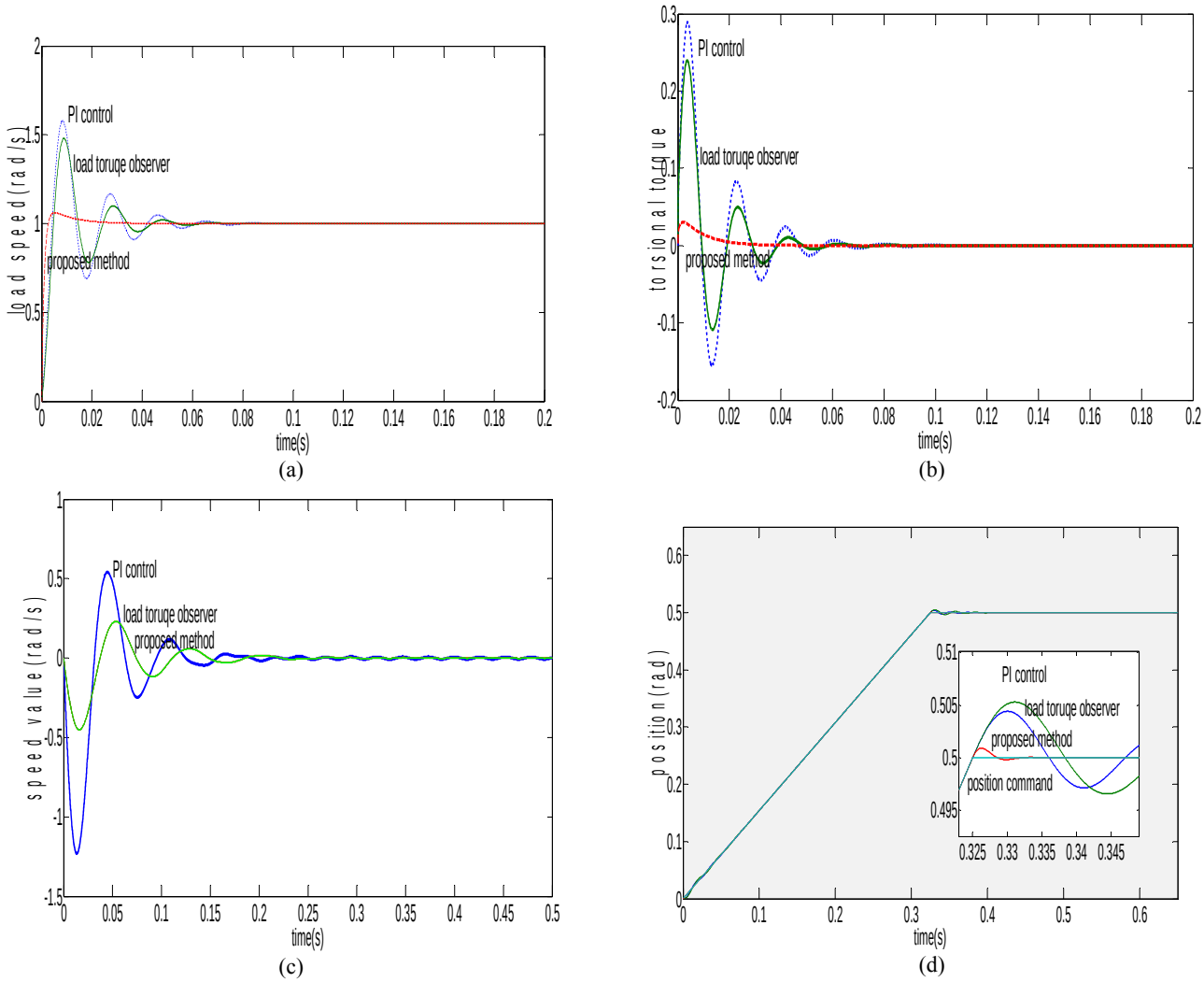

Fig. 9. (a) Speed response under three different control systems. (b) Torsional torque under three different control systems. (c) Disturbance response under three different control systems. (d) Position tracking under three different control systems.

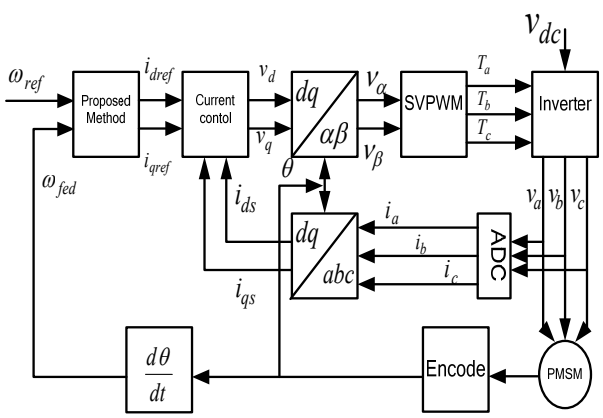

Fig. 10. Diagram of the software control unit.

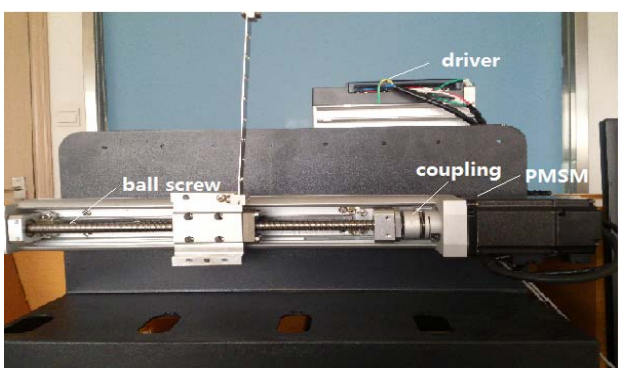

Fig. 11. Experimental platform.

three signals from up to down are command torque, motor feedback speed, and position error, respectively. From Fig. 13, the vibrations in position, torque, and speed last for a long time ($t > 125\ ms$) with the PI controller. Fig. 14 shows that the disturbance observer suppresses the vibration to a certain extent, but its performance is not as promising as the proposed method in Fig. 15. The vibration with the proposed method in Fig. 15 is nearly suppressed, and the positioning time is only $t \approx 69\ ms$. These experimental results have the same tendency as the simulation results. Disturbance

TABLE III
PMSM PARAMETERS

Paramater	Value	Unit
V_N	220	v
P_N	400	w
J_m	0.027×10^{-3}	$Kg.m^2$
I_N	2.0	A
n_N	3000	r/min
T_N	1.27	N.m

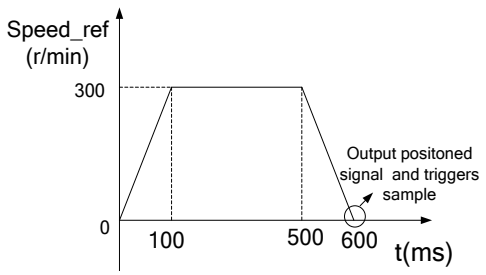

Fig. 12. Command speed wave.

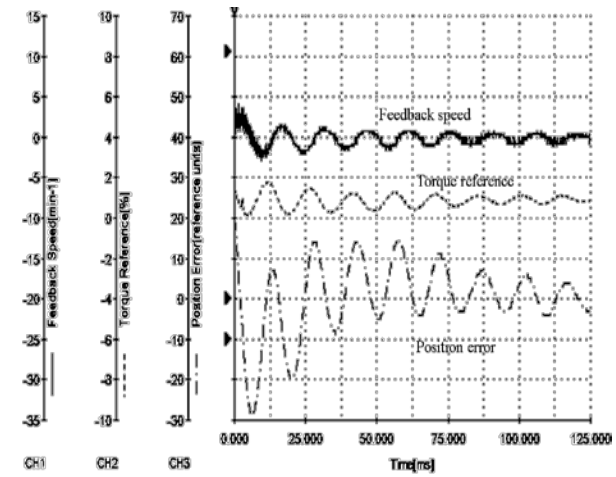

Fig. 13. Results of the PI controller.

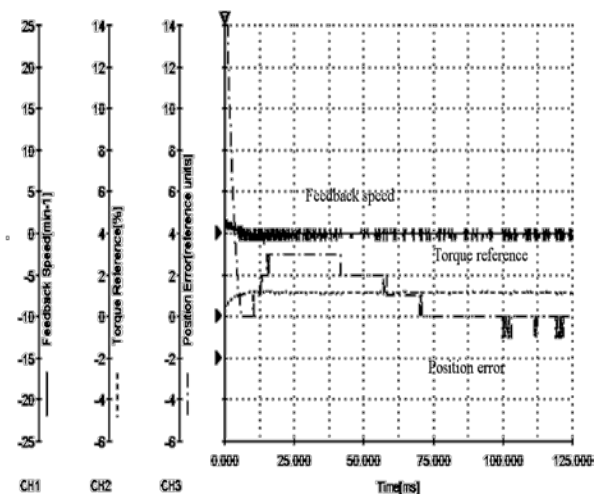

Fig. 14. Results of the disturbance torque observer.

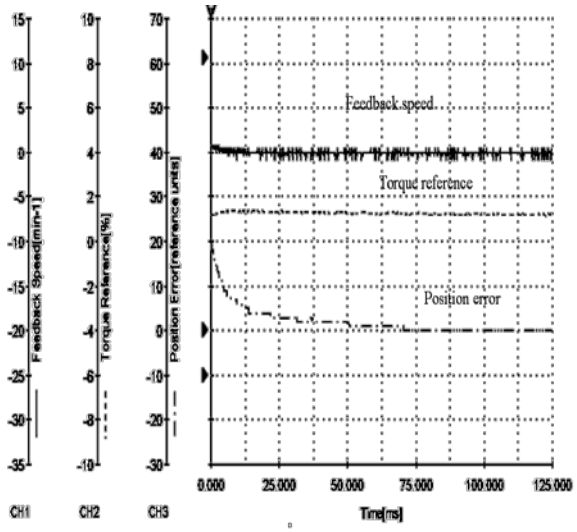

Fig. 15. Results of the proposed method.

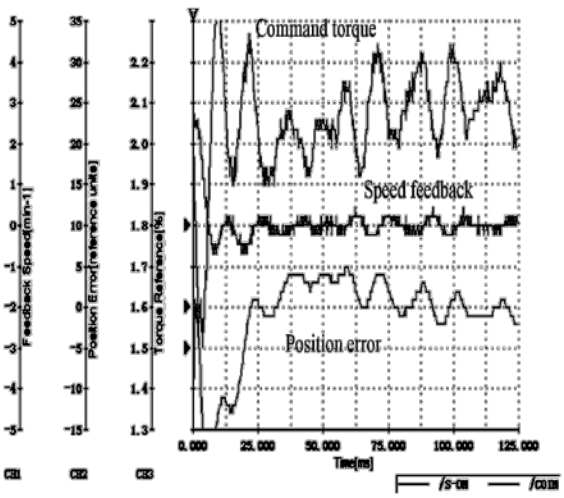

Fig. 16. Disturbance experimental results of the PI controller.

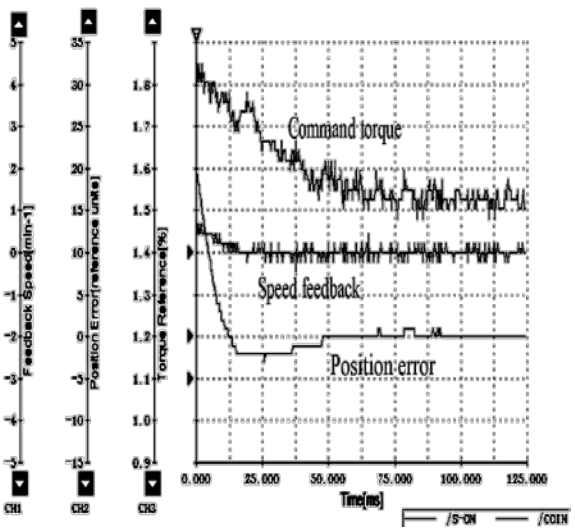

Fig. 17. Disturbance experimental results of the proposed method.

rejection experiments are also performed. We apply inconsiderable disturbance torque on the load side suddenly after the fixing position. The experimental results are described in Figs. 16 and 17. Fig. 16 shows that, with the PI controller, the torque, speed, and position vibrate because of the disturbance. By contrast, the corresponding signals rapidly return to the stable value with the proposed method in Fig. 17. This result is in accordance with the simulation results in Fig. 9(c). In conclusion, the proposed method performs better than the PI controller in command response and has better disturbance rejection capability.

VI. CONCLUSION

Vibration suppression is crucial for industrial applications. This paper presents a vibration suppression strategy based on torque feed-forward compensation and disturbance observer for a two-mass system. The control parameters K_P, K_I and ω_{cf}, K_G are designed by using a few system parameters (J_m, J_L, K_s) based on the CDM. A low-order Luenberger disturbance observer is applied to improve the disturbance rejection capability. The parameters of the disturbance observer are designed by analyzing the transfer function between motor speed and disturbance torque. We also analyze the transfer functions between load speed and speed command under both PI control and the proposed method. The bode diagrams explain how the proposed method can suppress vibration in theory. The proposed method offsets the resonance peak. Hence, the system should be stable at the resonance point. The simulation analysis and experimental results verify the good performance of the proposed method.

REFERENCES

[1] M. Hirata, K. Z. Liu, and T. Mita, "Active vibration control of a 2-mass system using u-synthesis with a descriptor from representation ." *Control Eng, Pract*, Vol. 4, No. 4, pp. 545 -552, Apr. 1996.

[2] S. N. Vukosavic and M. R. Stojic, "Suppression of torsional oscillations in a high-performance speed servo drive," *IEEE Trans Ind. Electron*., Vol. 45, No. 1, pp. 108-117, Feb. 1998.

[3] R. Musznski and J. Deskur, "Damping of torsional vibration in high-dynamic industrial drives," *IEEE, Trans. Ind. Electron*, Vol. 57, No. 2, pp. 554-552, Feb. 2010.

[4] L. Wang and Y. Frayman, "A dynamically generated fuzzy neural network and its application to torsional vibration control of tandem cold rolling mill spindles," *Eng. Appl. Artif. Intell.*, Vol. 15, No. 6, pp. 541-550, Dec. 2002.

[5] T. Orlowska-Kowalska and K. Szabat, "Neuro-fuzzy approach for mechanical variables estimation of a two-mass drive system," *IEEE Trans, Ind. Electron*, Vol. 54, No. 3, pp. 1352-1364, Jun. 2007.

[6] T. Orlowska-Kowalska, M. Dybkowski, and K. Szabat, "Adaptive sliding-mode neuro-fuzzy control of the two-mass drive system," *IEEE Trans. Ind. Electron.*, Vol. 54, No. 3, pp. 1352-1364, Jun. 2007.

[7] R. Dhaoudi, K. Kubo, and M. Tobise, "Two-degree of-freedom robust speed controller for high-performance rolling mill drives." *IEEE Trans. Ind. Appl.*, Vol. 29, No. 5, pp. 919-926, Sep./Oct. 1993.

[8] K. Sugiura and Y. Hori, "Vibration suppression on 2-and 3-mass system based on the feedback of imperfect derivative of the estimated torsional torque," *IEEE Trans. Ind. Electron*., Vol. 43, No. 1, pp. 56-64, Feb. 1996.

[9] A. V. Lipatov and N. I. Sokolov, "Some suficient conditions for stability and instability of continuous linear stationary systems," *Automatic Remote Control*, 1979, pp. 1285-1291, translated from Automaticka, iTelemekha-nika, No. 9, pp. 30-37, 1978.

[10] R. W. Hejny and R. D. Lorenz, "Evaluating the practical low-speed limits for back-EMF tracking-based sensorless speed control using drive stiffness as a key metric," *IEEE Trans. Ind. Applicat.*, Vol. 47, No. 3, pp. 1337-1343, May/Jun. 2011.

[11] S. Manabe, "Sufficient condition for stability and instability by Lipatov and its application to be coefficient diagram method." *9th Workshop on Astrodynamics and Flight Mechanics, ISAS*, 1999.

[12] S. Manabe, "The coefficient diagram method," *14th IFAC Symposium on Automatic control in Aerospace*, 1998.

[13] S. Manabe, "Application of coefficient diagram method to MIMO system," *10th Workshop on Astrodynamics and Flight Mechanics, ISAS*, 2000.

[14] A. Bahr and S. Beineke, "Mechanical resonance damping in an industrial servo drive," *IEEE European Conf., Power Elec. and Appl.*, pp.1-10, 2007.

[15] H. Kawaharada, I. Godler, T. Ninomiya, H. Honda, "Vibration suppression control in 2-inertia system by using estimated torsion torque," *IEEE IECON*, Vol. 3, pp. 2219-2224, 2000.

[16] Y. C. Kim, L. H. Keel, and S. P. Bhattacharyya, "Transient response control via characteristic ratio assignment," *IEEE Trans, Autom. Control*, Vol. 48, No. 12, pp. 2238-2244, Dec. 2003.

[17] S. Manabe, "Controller design of two-mass resonant system by coefficient diagram method," *T. IEE Japan*, Vol. lI8-D, No. 1, pp. S8-66, 1998.

[18] S. E. Saarakkala and M. Hinkkanen, "State-space speed control of two-mass mechanical systems: Analytical tuning and experimental evaluation," *IEEE Trans. Ind. Appl.,* Vol. 50, No. 5, pp. 3428-3437, Sep./Oct. 2014.

[19] S. E. Saarakkala, T. Leppinen, M. Hinkkanen, and J. Luomi, "Parameter estimation of two-mass mechanical loads in electric drives," *Advanced Motion Control (AMC), 2012 12th IEEE International Workshop on*. pp. 1-6, 2012.

[20] I. U. Khan and R. Dhaouadi, " Robust control of elastic drives through immersion and invariance," *IEEE Trans. Ind. Electron.,* Vol. 62, No. 3, pp. 1572-1580, Oct. 2014.

[21] K. Szabat, T. Tran-Van, and M. Kaminski, "A modified fuzzy luenberger observer for a two-mass drive system," *IEEE Trans. Ind. Informat.,* Vol. 11, No. 2, pp. 531-539, Jun. 2014.

[22] J.-S. Ko, Y.-G. Seo, and H.-S. Kim, "Precision position control of PMSM using neural observer and parameter compensator," *Journal of Power Electronics*. Vol. 8, No. 4, pp. 354-362, Oct. 2008.

Qiong Li was born in China in 1989. She received her B.S. in Electrical Engineering from East China Jiaotong University, Jiangxi, China. She is currently working toward her Ph.D in Electrical Engineering from Huazhong University of Science and Technology, Wuhan, China. Her current research interests include high-performance servo drivers and control of robots in industrial fields.

Qiang Xu was born in China in 1968. He received his B.S., M.S., and Ph.D. in Electrical Engineering from Huazhong University of Science and Technology, Wuhan, China. He is currently a professor at the Department of Electrical Engineering. His current research interests include high-performance servo drivers and control of robots in industrial fields.

Ren Wu was born in China in 1987. He received his B.S. in Electrical Engineering from Shenyang University of Technology, Shenyang, China. He is currently working toward his Ph.D in Electrical Engineering from Huazhong University of Science and Technology, Wuhan, China. His current research interests include the design of high-efficiency permanent-magnet synchronous motors and the control of servo drivers.